Effects of Temperature, Photoinjection, and Magnetic Field on the Photomagnetoelectric Response in As-Doped Si†

SHENG-SAN LI
Electrical Engineering Department, University of Florida, Gainesville, Florida 32601
(Received 1 April 1969; revised manuscript received 28 July 1969)

Photomagnetoelectric (PME) and photoconductive (PC) effects in As-doped Si ($N_d=1.4\times10^{16}$ cm^{-3}) have been investigated as functions of temperature (7.9°K–27°K), photoinjection, and magnetic-field strength (0–8000 G). The high-injection electron lifetime (τ_{n0}), ambipolar diffusion length, ambipolar diffusivity, and effective carrier mobility are deduced from the experimental data on the PME open-circuit voltage, photoconductance, and the Hall coefficient. The Shockley-Read model is used to interpret the recombination and trapping mechanism involved. It is found that the defect density in this sample is approximately equal to 5.6×10^{12} cm^{-3}, and the defect level is believed to be acceptor-type and located in the lower half of the band gap. The electron-capture cross section is found equal to 6.5×10^{-15} cm^{-3} at 20°K and 2.18×10^{-15} cm^{-3} at 24°K. The experimental results for V_{PME}, I_S, and G versus magnetic field are found in good agreement with theory for $T\geqslant20$°K and for the high-injection region. Deviations of the results from theory at high magnetic fields are observed for $T\leqslant14$°K and for the moderate-injection region.

INTRODUCTION

SINCE the discovery of the photomagnetoelectric (PME) effect in Cu_2O by Kikoin, Noskov, and Croetzinger[1,2] studies of the PME effect have been made for Bi, Te, InSb, PhS, Ge, and Si.[3–9] The most comprehensive theory of the general PME effect at low magnetic fields is from to Van Roosbroeck.[10]

Bulliard[11] initially verified the existence of the PME effect in Si. Garreta and Grosvalet[12] calculated minority-carrier lifetimes for two samples of Si at 300°K. Mette and Boatwright[13] utilized the PME effect to investigate surface recombination speeds in thin p-type Si of 200 Ω cm, also at 300°K. Barker[14] has commented on the results of Mette and Boatwright and postulated a simple photodissociation model to account for the sublinear response of the PME-voltage-versus-illumination intensity.

In our recent paper[15] we have reported the measurements of the PME and PC effects in phosphorus-doped Si containing a donor concentration of 1.13×10^{17} cm^{-3} at $T=21.8$°K. The results indicated that concurrent measurements of the PME, PC and Hall effects in a silicon sample at low temperatures may yield the recombination and transport parameters such as carrier lifetime, ambipolar diffusion length, and effective carrier mobility. Since at low temperature the PME and PC responses in silicon are relatively sensitive to the temperature, a study of the temperature dependence of the PME and PC responses in silicon may yield some conclusive results regarding the recombination and the transport properties in silicon at low temperatures. The main objective of this paper will therefore be concerned with the effects of the temperature, photoinjection, and magnetic field on the PME open-circuit voltage, PME short-circuit current, and the photoconductance for the arsenic-doped silicon, between 7.9 and 27°K. Of particular interest in this work is the study of the PME apparent lifetimes as functions of photoinjection and temperature. The Shockley-Read (SR) model[16] is used to interpret the recombination and trapping effects in this sample. Conclusions are reached from the PME and the PC measurements on As-doped Si. The results for the PME and PC responses versus magnetic field are in accord with theoretical predictions for $T>20$°K and for the high-injection region. However, deviations of these results from theory are observed for $14°>T>7.9$°K and for the moderate-injection region, particularly at high magnetic fields. This has been interpreted as a result of the increase in carrier lifetimes with decreasing photoinjection. The electron-capture cross section is deduced from PME apparent lifetime, using the SR model.

THEORY

A general treatment of the steady-state PME and PC theory under the conditions of high photoinjection (i.e., $\Delta n=\Delta p\gg n_0$) and arbitrary magnetic field strength has been developed in our previous paper[15] and will not be

† Research supported by the Advanced Research Projects Agency, U. S. Department of Defense, and monitored by the Air Force Cambridge Research Laboratories under Contract No. F 19628-68-(C)-0058.

[1] K. Kikoin and M. Noskov, Physik Z. Sowjetunion **5**, 586 (1934).
[2] G. Groetzinger, Z. Physik. **5**, 36 (1934); **5**, 169 (1934).
[3] P. Aigrain and H. Bulliard, Compt. Rend. **236**, 595 (1953); **236**, 672 (1953).
[4] H. Bulliard, Ann. Phys. (N. Y.) **9**, 52 (1954).
[5] T. S. Moss, L. Pinchere, and A. M. Woodward, Proc. Phys. Soc. (London) **B66**, 743 (1953).
[6] T. S. Moss, Proc. Phys. Soc. (London) **B66**, 993 (1953).
[7] S. W. Kurnick and R. N. Zitter, J. Appl. Phys. **27**, 278 (1956).
[8] R. N. Zitter, Phys. Rev. **112**, 852 (1958).
[9] R. N. Zitter, A. J. Strauss, and A. E. Attard, Phys. Rev. **115**, 266 (1959).
[10] W. Van Roosbroeck, Phys. Rev. **101**, 1713 (1956).
[11] H. Bulliard, Phys. Rev. **94**, 1564 (1959).
[12] O. Garreta and J. Grosvalet, in *Progress in Semiconductors*, edited by A. F. Gibson (John Wiley & Sons, Inc., New York, 1956), Vol. I, p. 167.
[13] H. L. Mette and A. Boatwright, Phys. Rev. **140**, A919 (1965).
[14] R. E. Barker, Jr., Phys. Rev. **149**, 663 (1966).
[15] S. S. Li and C. Wang, in Proceedings of the Third International Conference on Photoconductivity, 1969 (unpublished).
[16] W. Shockley and W. T. Read, Phys. Rev. **87**, 835 (1952).

TABLE I. Recombination and transport parameters for As-doped silicon.

Temperature	300°K	27°K	24°K	20.4°K	11°K	7.9°K
Electron density n_0 (cm^{-3})	1.4×10^{16}	2.63×10^{11}	5.8×10^{10}	8.8×10^{9}	5.1×10^{9}	4.2×10^{9}
Hall mobility μH (cm^2/V sec)	0.12×10^{4}	2.37×10^{4}	2.4×10^{4}	2.6×10^{4}	2.39×10^{4}	2.43×10^{4}
Ambipolar diffusivity D (cm^2/sec)	21	37	33.4	30.6	15	4.58
Ambipolar diffusion length L (cm)		2.28×10^{-2}	1.73×10^{-2}	1.45×10^{-2}	0.95×10^{-2}	0.17×10^{-2}
High-injection electron lifetime τ_{n0} (μsec)		14	8.54	6.21	0.71	0.58
Electron-capture cross section σ_n (cm^2)			2.18×10^{-15}	6.5×10^{-15}		

repeated here. Only those expressions which are pertinent to the present case will be presented here.

Theoretical expressions for PME open-circuit voltage, PME short-circuit current, and the photoconductance given below are obtained under the assumptions that (1) $\Delta n=\Delta p\gg n_0$, (2) $d>4L$, and (3) $s_1\gg s_2$. Assumption (1) is found satisfied in regions I and II, as will be shown later; assumptions (2) and (3) are satisfied for the present sample.

The PME open-circuit voltage per unit length $V_{\rm PME}$ is given by[15]:

$$V_{\rm PME}=\left(\frac{D}{\tau}\right)^{1/2}\frac{B}{(1+\mu^2B^2)^{1/2}}, \tag{1}$$

where $\mu=(\mu_n\mu_p)^{1/2}$, and D is the ambipolar diffusion constant. Equation (1) predicts that $V_{\rm PME}$ is directly proportional to B at low fields and reaches a constant value at high magnetic fields. If the carrier lifetime τ is constant, then $V_{\rm PME}$ will be independent of the illumination intensity (or photoinjection).

The photoconductance per unit width G as a function of the magnetic field is given by the expression

$$G=\frac{eI_0(1+b)}{\sqrt{b}}\frac{\mu}{s_1}\frac{(D\tau)^{1/2}}{(1+\mu^2B^2)^{1/2}}. \tag{2}$$

Equation (2) predicts that G is insensitive to B at low fields and is inversely proportional to B for $\mu B>1$. It further shows that G is also a function of illumination intensity I_0, carrier lifetime τ, and the surface velocity s_1.

The PME short-circuit current per unit width, I_s, can be derived independently or obtained from the products of Eqs. (1) and (2). The result reads

$$I_s=\frac{e(1+b)I_0}{\sqrt{b}}\frac{\mu B}{(1+\mu^2B^2)}\frac{D}{s_1}. \tag{3}$$

Equation (3) predicts that I_s is directly proportional to B at low fields; it passes the maximum at $\mu B\simeq1$ and then decreases with B for $\mu B>1$.

By comparison of Eqs. (1)–(3), one obtains the expression

$$I_s=V_{\rm PME}G, \tag{4}$$

which shows that I_s may be obtained from $V_{\rm PME}$ and G.

SAMPLE PREPARATION AND MEASUREMENT TECHNIQUE

An arsenic-doped (1.4×10^{16}-cm^{-3}) silicon wafer was cut into a rectangular slab with a diamond saw. The dimensions of the slab are $0.1\times0.4\times1$ cm. The surfaces were first lapped with 600- and 1000-grit abrasive powders to remove saw marks.

The sample was then prepared for the electrodeless plating of nickel to provide low-resistivity Ohmic contacts. The portion of the slab to be illuminated was etched with CF_4 to provide low surface-recombination speed, and the dark side of the slab was sandblasted to achieve high surface-recombination speed.

Following etching, the electric wires and the thermocouples were soldered to the sample, and the sample was then attached to the "cryotip" of the AC-3L refrigeration system. The sample chamber was then evacuated down to 10^{-4}–10^{-5} Torr by mechanical and diffusion pumps to prevent deterioration of the etched surface.

In order to obtain strong illumination intensity, a 650-W tungsten lamp incorporated with two focusing lenses and a 15-cm water filter were employed. It was found that the long-wavelength photons ($\lambda>1.1\ \mu$) and the thermoelectric effect were effectively removed by the water filter.

A calibrated gold-iron-copper thermocouple wire was used to monitor the temperatures below 100°K. A 6-in. Varian electromagnet with field-sweep units was used to achieve the required field intensity.

The PME open-circuit voltage was measured as a function of the magnetic field, using an X-Y recorder. A constant current source was employed for photoconductance and Hall-effect measurements. Precautions were taken to minimize the possible experimental errors.

RESULTS AND ANALYSIS

Experimental results of the PME and PC responses, electrical resistivity and Hall coefficient measured at

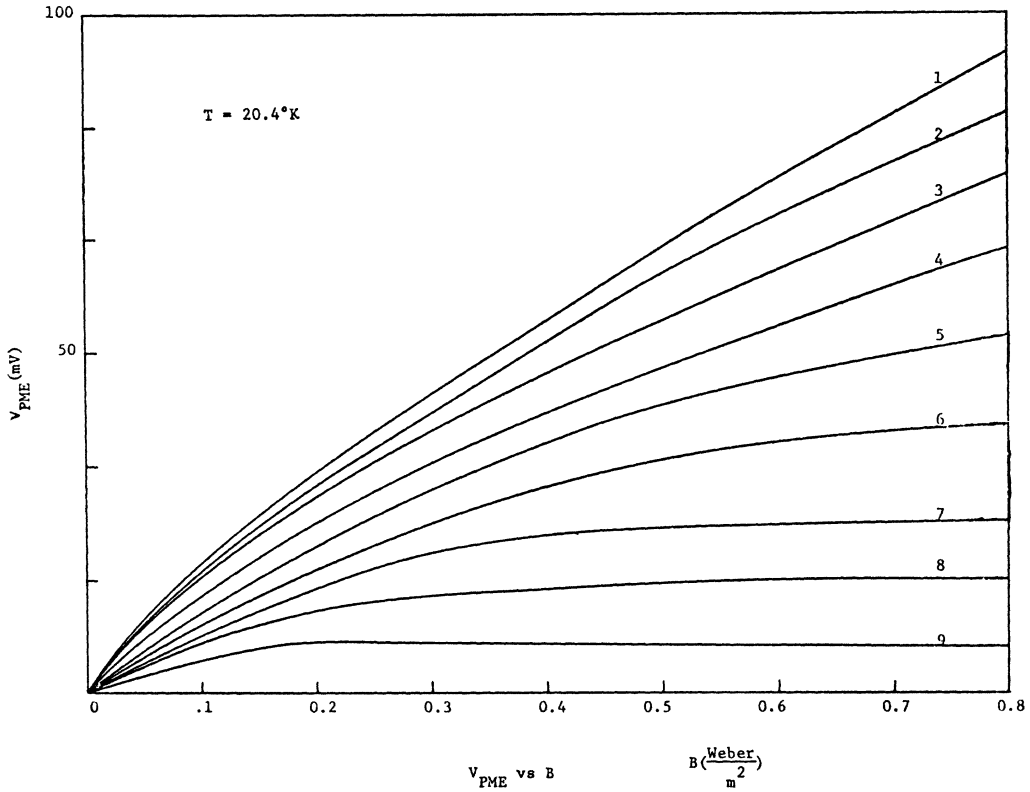

FIG. 1. PME open-circuit voltage V_{PME} versus magnetic field B with relative photoconductance G/G_0 as parameter for $T=20.4$°K. Curve 1 denotes $G/G_0=2070$; 2, 1865; 3, 1560; 4, 1340; 5, 1130; 6, 860; 7, 420; 8, 138.

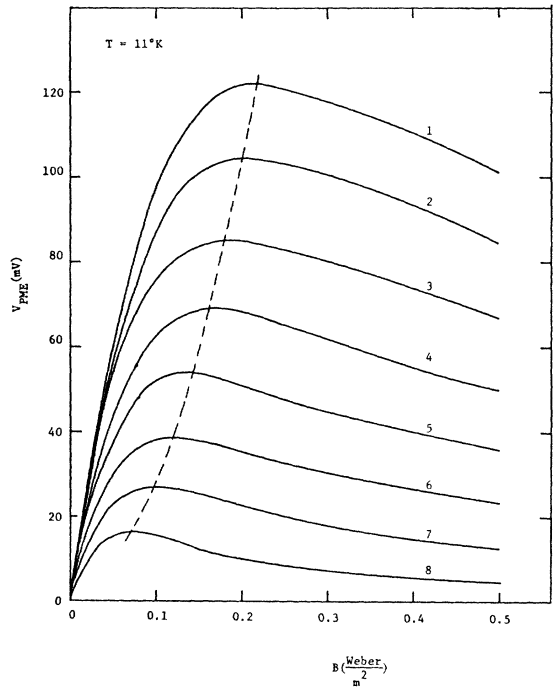

FIG. 2. PME open-circuit voltage V_{PME} versus magnetic field B with relative photoconductance G/G_0 as parameter for $T=11$°K. Curve 1 denotes $G/G_0=316$; 2, 280; 3, 244; 4, 213; 5, 184; 6, 158; 7, 130; 8, 106.

7.9, 11, 14, 20.4, 24, and 27°K are presented and analyzed in detail. For comparison, the transport and recombination parameters deduced from these measurements are summarized in Table I. The equilibrium electron concentrations determined from the Hall coefficient below 20°K are higher than theoretical predictions, due to background radiation. The Hall mobility determined from the Hall and resistivity measurements is found insensitive to the temperature between 7.9 and 27°K, which implies that the acoustic lattice and the impurity scattering may play the same important role over this temperature range. The ambipolar diffusivity is deduced from the Hall mobility, using the Einstein relation and assuming an electron-hole mobility ratio of 2.

The average photoinjected excess carrier density, Δn, is calculated from the measured photoconductance for different illumination intensities, using the approximation

$$\Delta n/n_0 \simeq (G/G_0)b/(b+1). \tag{5}$$

The ambipolar diffusion length and the high-injection lifetime can be deduced from the PME open-circuit voltage under high-injection and low-magnetic-field conditions. The PME open-circuit voltage per unit length for this case is given by

$$V_{PME}=(D/\tau)^{1/2}B. \tag{6}$$

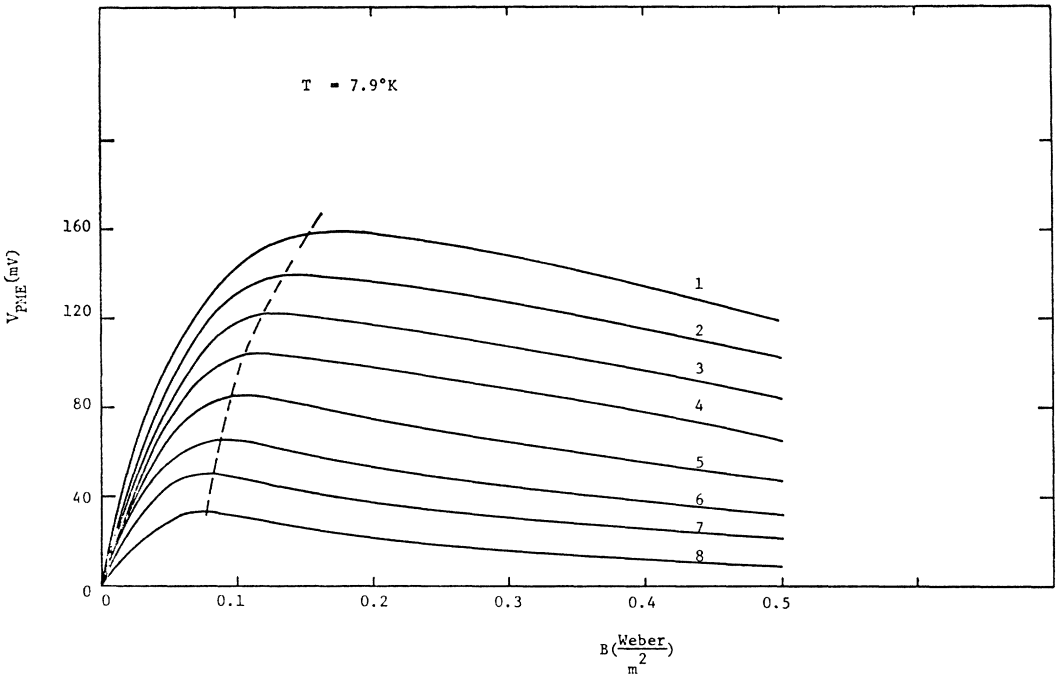

FIG. 3. PME open-circuit voltage V_{PME} versus magnetic field B with relative photoconductance G/G_0 as parameter for $T=7.9$°K. Curve 1 denotes $G/G_0=192$; 2, 155; 3, 130; 4, 109; 5, 88; 6, 48; 7, 55; 8, 40.

The effective carrier mobility can also be obtained from the V_{PME} at high magnetic fields,

$$V_{PME}=(D/\tau)^{1/2}/\mu, \quad \text{for} \quad \mu B>1. \tag{7}$$

Figures 1–3 illustrate the plots of V_{PME} versus B, with the illumination intensity as parameter, for $T=20.4$, 11, and 7.9°K. From Fig. 1, it is found that the curves of V_{PME} versus B are in accord with theoretical predictions by Eq. (1) for $T=20.4$ °K. The PME apparent lifetime τ can be evaluated at low magnetic fields, using Eq. (6). The effective carrier mobility in Eq. (7) is calculated at high magnetic fields in which V_{PME} is constant. It is found that the effective carrier mobility μ at 20.4°K varies from 3.2–1.9×10^4 cm²/V sec, as the photoinjection is increased. The PME open-circuit voltage is directly proportional to the magnetic field at low fields and reaches a constant value at high magnetic fields. It is interesting to note that the peak of this plot is shifted to high-field region as the photoinjection is increased, which indicates that the effective carrier mobility is decreased with increasing photoinjection. This is due to the fact that between 4.2 and 27°K, most of the electrons are frozen out on the arsenic site, the increase in the photoinjection denuding the neutral arsenic atoms and thus making the ionized-impurity scattering more effective. The same results (shifting of the peak to the right) are also observed at 7.9 and 11°K, as can be seen from Figs. 2 and 3. However, the results of V_{PME} versus B observed at 7.9 and 11°K deviate from theoretical predictions at high magnetic fields.

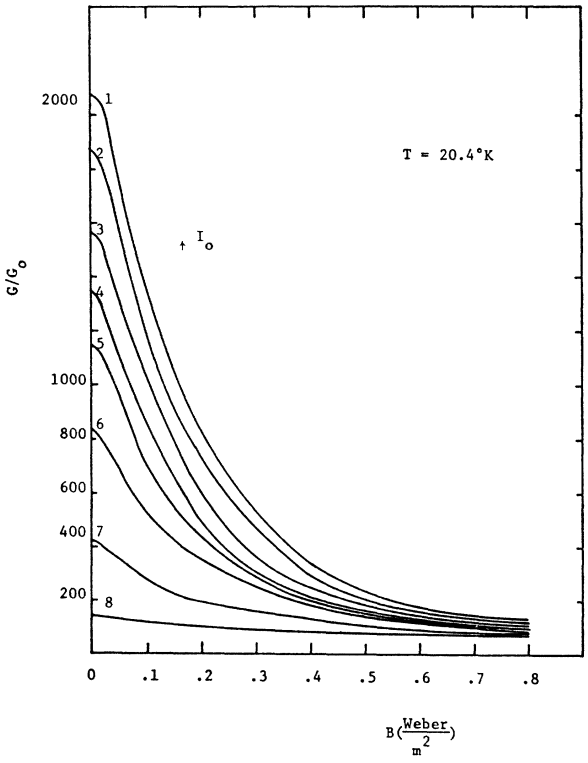

FIG. 4. Relative photoconductance G/G_0 versus magnetic field B with illumination intensity I_0 as parameter for $T=20.4$°K.

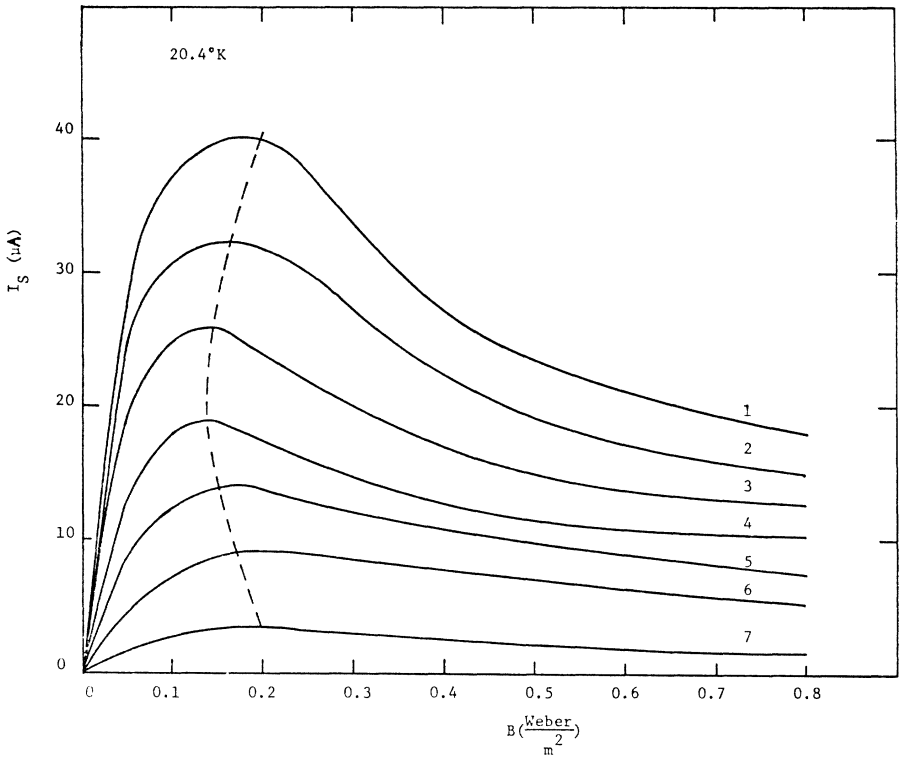

FIG. 5. PME short-circuit current I_s versus magnetic field B with relative photoconductance as parameter for $T=20.4$°K. This plot is obtained from Figs. 1 and 4.

The results show that the PME open-circuit voltage increases linearly with B at low fields and reaches a maximum value at a certain field strength and then decreases slowly with further increase in magnetic field. The decrease in V_{PME} at high magnetic fields indicates that the effective carrier lifetime τ is increased with magnetic fields, which in turn causes the decrease of V_{PME} with B [see Eq. (1)]. The increase of τ with B can be interpreted alternatively from the fact that G is decreased with increasing B, and the decrease in G causes the increase in τ. This will become clarified when we introduce the plot of carrier lifetime versus excess carrier density, which will be discussed later. In Fig. 4, the relative photoconductance G/G_0 is plotted as a function of magnetic field B, with illumination intensity as parameter, for $T=20.4$°K. The results indicate that at very high illumination intensity, the results are in accord with the theoretical predictions by Eq. (2), which predicts that G is approximately constant at low fields and is inversely proportional to B at high fields ($\mu B>1$). The deviations from the theoretical predictions for the moderate-injection region is again due to the increase of carrier lifetime with decreasing photoinjection in this region (note that $G\propto\sqrt{\tau}$). The maximum photoconductance observed at 20.4 °K for this sample is approximately 2000 G_0.

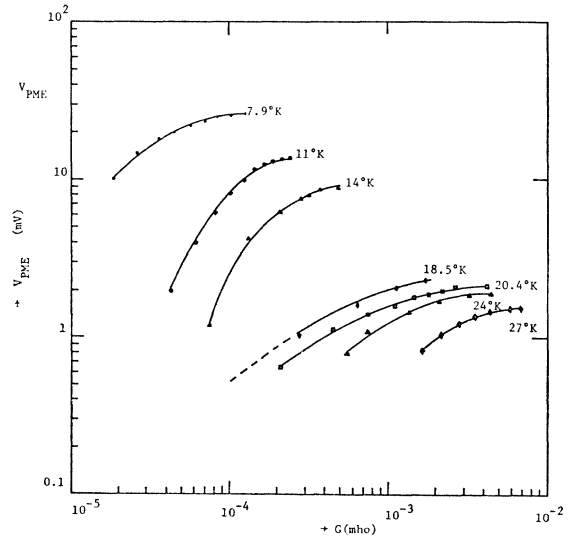

FIG. 6. PME open-circuit voltage V_{PME} versus photoconductance for various temperatures. The results show that V_{PME} decreases with increasing temperature.

Figure 5 demonstrates the PME short-circuit current I_s versus magnetic field, with illumination intensity as parameter, for $T=20.4$°K. This plot is obtained from Figs. 1 and 4, using Eq. (4). The results show that the I_s-versus-B curves for the high-injection region are in accord with theoretical predictions by Eq. (3). However, for moderate injection, the results deviate from theory; the peak of the I_s-versus-B curves tends to flatten out and approaches a constant value at high magnetic fields. This is again due to the fact that G is essentially

independent of B in the moderate-injection region (see Fig. 4).

Figure 6 illustrates the PME open-circuit voltage versus photoconductance with temperature as parameter and for $B=0.01$ Wb/m^2. The results show that (1) the V_{PME} increases as the temperature is decreased, (2) the V_{PME} increases with increasing photoinjection and reaches a constant value at very high-injection levels, implying that τ is decreased with increasing photoinjection ($V_{\mathrm{PME}} \propto \tau^{-1/2}$), (3) the V_{PME} increases faster with G, between 7.9 and 14°K, than those between 18.5 and 27°K, which implies that τ changes more rapidly with photoinjection at $T=7.9$ and 14°K than for $27>T>20$°K.

Figure 7 displays the PME short-circuit current I_s versus the photoconductance G with temperature as parameter and for $B=0.01$ Wb/m^2. It is noted that the I_s-versus-G curve shifts to the left (or low-photoconductance region) as temperature is decreased (except at 27°K). Three distinctive regions are observed from this plot over the entire measuring temperature range 7.9–27°K: (1) very high-injection region (region I): in this region I_s is directly proportional to G, and τ is essentially constant and equals the high-injection lifetime ($\tau=\tau_{n0}+\tau_{p0}$); (2) high-injection region (region II); in this region I_s varies in proportion as $G^{5/4}$, and τ varies in proportion as $\Delta n^{-1/2}$; (3) moderate-injection region (region III); in this region I_s varies with G^r($r\cong 2$ to 2.5), and τ is a strong function of photoinjection; the effect of trapping predominates in this region.

In Fig. 8 the PME apparent lifetime τ is plotted as a function of the photoconductance G, with temperature as parameter; the PME lifetime was deduced from the PME open-circuit voltage at $B=0.01$ Wb/m^2 and for different illumination intensities. The results indicate that τ decreases with increasing photoinjection and reaches a constant value at very high-injection levels. The results also indicate that the high-injection lifetime τ_∞ decreases as temperature is decreased. From the curve-fit of Fig. 9 it is found that

$$\tau_\infty \cong \tau_{n0} \cong 3.68\times 10^{-9} T^{2.5}. \tag{8}$$

Since the effective lifetime decreases with increasing injection, we assumed that the flaw levels are to be acceptor type and in the lower half of the band gap, then the τ_∞ will be approximately equal to τ_{n0} (since $\sigma_p \gg \sigma_n$). From the above expression, it is also found that the capture cross section will increase with decreasing temperature between 27 and 7.9°K. The short high-injection lifetime observed in this sample as compared to that of the phosphorus-doped silicon reported previously,[15] indicates that the flaw density in this sample is higher than that of the phosphorus-doped silicon sample.

The electron lifetime for small injection and for arbitrary flaw density N_f is given by [17]

$$\tau_n = \tau_0 \cong \tau_{n0}[(p_1+N_f)/n_0], \tag{9}$$

for N_f in the lower half of the band gap.

From Fig. 8, it is seen that the PME apparent lifetime τ increases rapidly as the photoinjection is

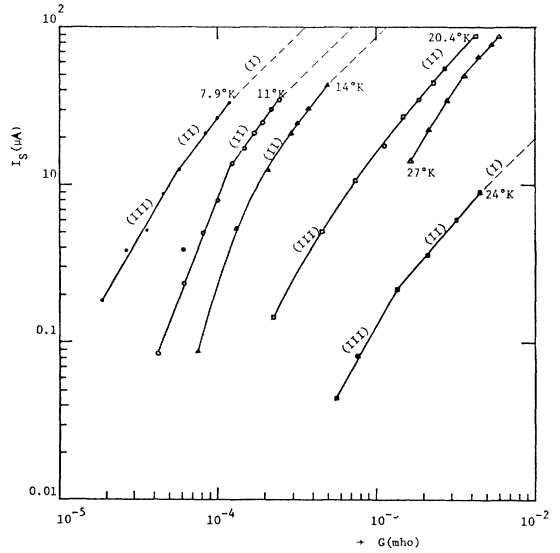

FIG. 7. The PME short-circuit current I_s versus photoconductance G for different temperatures. Three distinctive regions are obtained for each temperature: region I, $I_s \propto G$; region II, $I_s \propto G^{5/4}$, and region III, $I_s \propto G^r$ ($r=1.6$–2.3).

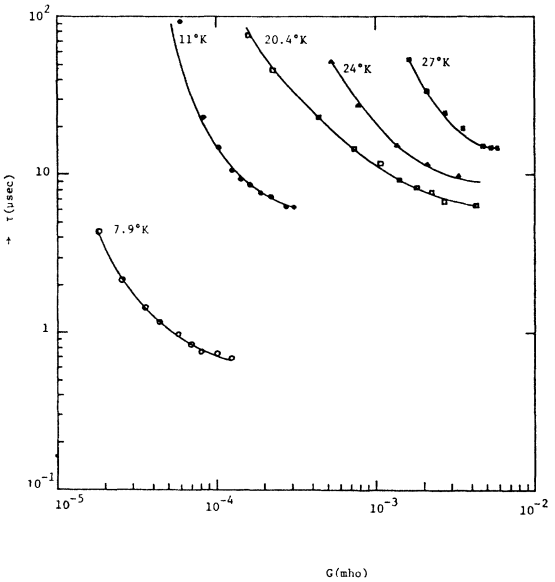

FIG. 8. PME apparent lifetime τ is plotted as a function of photoconductance with temperature as parameter. At very high injection, τ approaches the high-injection electron lifetime τ_{n0} which is found to decrease with decreasing temperature.

[17] J. S. Blakemore, *Semiconductor Statistics* (Pergamon Press, Inc., New York, 1962).

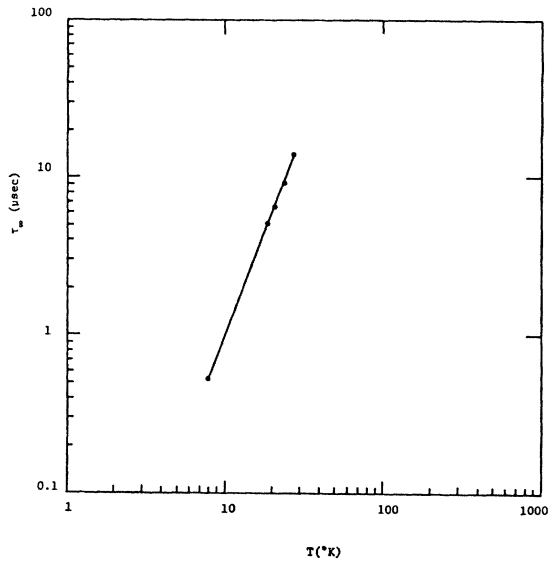

FIG. 9. High-injection lifetime τ_∞ is plotted as a function of temperature. Using curve fit, τ_∞ is found equal to 3.68×10^{-9} $T^{2.6}$ μsec.

decreased. This implies that the flaw density N_f is larger than the equilibrium electron concentration n_0 (since $\tau_n \gg \tau_{n0}$).

Figure 10 illustrates the PME apparent lifetime τ versus $\Delta n/n_0$ for $T=20.4$, 24, and 27°K. Note that in region I ($I_s \propto G$), τ reaches a constant value τ_∞, and in region II ($I_s \propto G^{5/4}$) the following relation between τ and Δn is found from the curve-fit of Fig. 9

$$\begin{aligned} \tau &= 1.96\times10^{-4}(\Delta n/n_0)^{-1/2}, \quad \text{at } 24°\text{K} \\ \tau &= 2.6\times10^{-4}(\Delta n/n_0)^{-1/2}, \quad \text{at } 20.4°\text{K} \end{aligned} \tag{10}$$

which are consistent with our previous results for phosphorus-doped silicon[15] (in which we observed regions I and II only).

In order to examine the validity of the simple model used in the derivation of high-injection PME and PC theory (we assumed that $\Delta n=\Delta p$ for the high-injection case), the Shockley-Read Model[16] is used to interpret the recombination and trapping mechanism in this sample. From the SR model, the effective carrier lifetime τ for n-type material can be expressed as a function of the excess carrier density for arbitrary modulation[17]:

$$\tau = \frac{\tau_0+\tau_\infty(\Delta n/n_0)}{(1+\Delta n/n_0)}, \tag{11}$$

where τ_0 is the zero modulation lifetime given by Eq. (9) and $\tau_\infty=\tau_{n0}$ for the assumed model. It is noted from Eq. (11) that a plot of $\tau(1+\Delta n/n_0)$ versus $\Delta n/n_0$ enables one to obtain the zero-modulation lifetime τ_0, provided that the effect of trapping is negligible. Figure 11 demonstrates the plot of $\tau(1+\Delta n/n_0)$ versus $\Delta n/n_0$ for $T=20.4$ and 24°K, using the apparent PME lifetime shown in Fig. 10. A striking linearity of this plot is obtained for $\Delta n/n_0$ exceeding 200 for both temperatures. This result indicates the adequacy of using the SR model to explain the recombination and trapping mechanism involved in this sample. The results indicate that in regions I and II the effect of trapping can be ignored, and thus the assumption that $\Delta n=\Delta p$ is valid for both regions. However, a large deviation from linearity was observed in the moderate-injection region ($\Delta n \cong 200 n_0$), indicating that the flaw density is large enough to make trapping serious in this region. The assumption that $\Delta n=\Delta p$ in our PME and PC theory[15] will no longer be valid for region III. To estimate the flaw density in this sample, the zero-modulation lifetime τ_0 is deduced from Fig. 11, which is given by

$$\begin{aligned} \tau_n &= \tau_0 = 4 \text{ msec}, \quad \text{at } 20.4°\text{K} \\ \tau_n &= \tau_0 = 1.4 \text{ msec}, \quad \text{at } 24°\text{K}. \end{aligned}$$

From the slope of the plot of $\tau(1+\Delta n/n_0)$ versus $\Delta n/n_0$, it is found that

$$\tau_\infty \cong \tau_{n0} = 4.14 \text{ μsec}, \quad \text{at } 20.4°\text{K}$$

and

$$\tau_\infty \simeq \tau_{n0} = 6.5 \text{ μsec}, \quad \text{at } 24°\text{K}.$$

Using Eq. (9) and assuming $p_1 \ll N_f$, the flaw density N_f is found to be approximately equal to 5.6×10^{12} cm^{-3}, which seems quite reasonable for the present results. The electron-capture cross section σ_n can be calculated from the expression

$$\sigma_n = 1/\tau_{n0} N_f v_{\text{th}}, \tag{12}$$

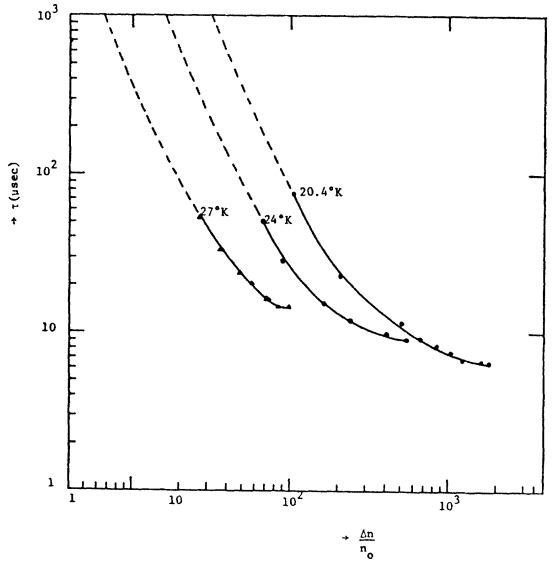

FIG. 10. PME apparent lifetime τ versus normalized excess carrier density $\Delta n/n_0$ for $T=20.4$, 24, and 27°K. In region II, τ is found to vary in proportion as $\Delta n^{-1/2}$, and in region I, τ is constant.

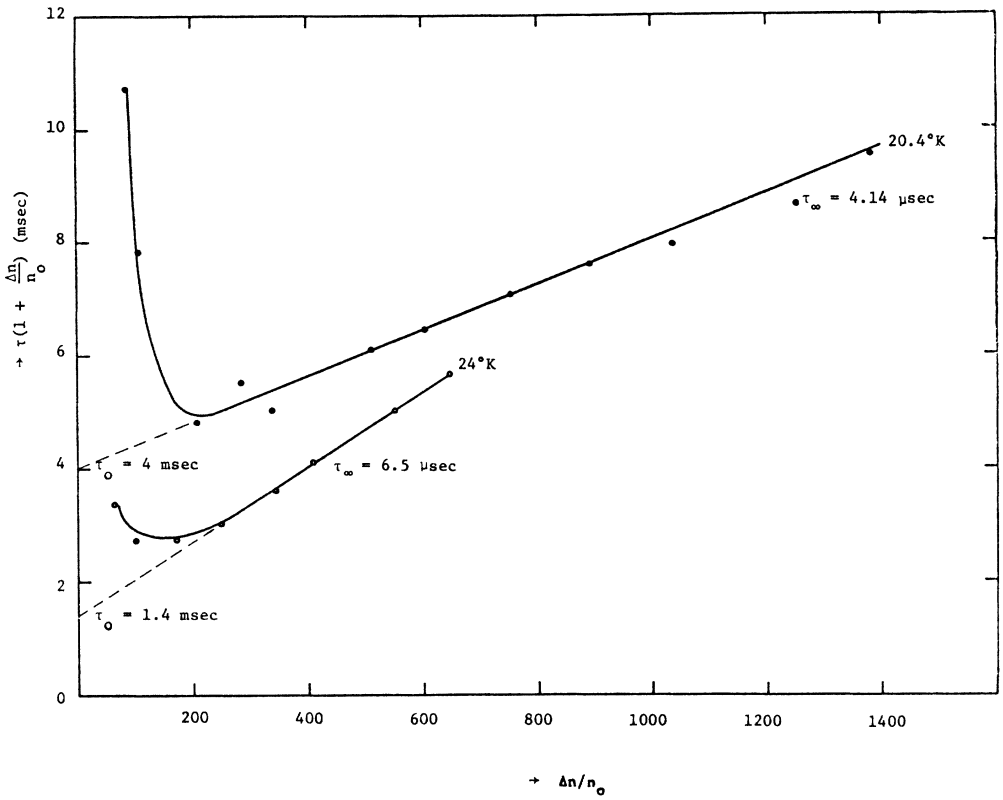

FIG. 11. $\tau(1+\Delta n/n_0)$ is plotted as a function of $\Delta n/n_0$ for $T=24$ and 20.4°K. A striking linearity is obtained for both curves for $\Delta n/n_0 > 200$. The slope of this straight line yields the high-injection lifetime τ_∞ and the intercept yields the zero-injection lifetime τ_0.

where v_{th} is the thermal velocity, and N_f is the flaw density which is equal to 5.6×10^{12} cm^{-3} for this sample. τ_{n0} is listed in Table I. The results for σ_n calculated at 20.4 and 24°K are given by

$$\sigma_n = 6.5\times10^{-15} \text{ cm}^2, \quad \text{at } 20.4°\text{K}$$

and

$$\sigma_n = 2.18\times10^{-15} \text{ cm}^2, \quad \text{at } 24°\text{K}.$$

Another interesting aspect regarding the effect of charge fluctuation in the arsenic levels on the relation between Δn and Δp has also been considered in this work. It is found from the charge-balance equation and the SR model that in regions I and II this effect can be completely ignored and the relation $\Delta n=\Delta p$ holds good for both regions (i.e., for $\Delta n > \Gamma_D N_D$).[18] However, for $n_0 < \Delta n < \Gamma_D N_D$ (region III), Δp is found equal to $(\Gamma_D N_D)^{-1}\Delta n^2$, which shows that holes are trapped in the arsenic-site levels. Application of the relation $\Delta p = (\Gamma_D N_D)^{-1}\Delta n^2$ to the PME and PC theory does not yield the correct prediction for I_s-versus-G curves at low magnetic fields and in the moderate-injection region (region III). It is therefore concluded that the effect of charge fluctuation in the arsenic levels on the trapping and recombination in this sample seems not significant as compared to that of the flaw levels located in the lower half of the band gap.

[18] This holds where $\Gamma_D=\sigma_{pD}/\sigma_{nD}$ is the ratio of electron-hole capture cross sections which is in the order of 10^{-3}–10^{-5} and $N_D \cong 10^{16}$ cm^{-3}.

DISCUSSION AND CONCLUSIONS

The PME and PC effects in the As-doped silicon have been measured and analyzed between 7.9 and 27°K. The recombination and transport parameters such as high-injection electron lifetime, electron-capture cross section, flaw density, ambipolar diffusion length, and the effective carrier mobility are deduced from the PME open-circuit voltage and the photoconductance data between 7.9 and 27°K. Some important results are summarized in Table I.

Conclusions regarding the trapping and the recombination mechanism as well as the effects of temperature, photoinjection, and magnetic field on the PME open-circuit voltage, carrier lifetime, and photoconductance are summarized as follows:

(1) It has been shown that experimental results for V_{PME}, I_s, and G versus magnetic field are in good agreement with the theoretical predictions for $27>T>20$°K and for injection regions I and II. However, for region III and for $7.9<T<14$°K, the results are de-

viated from the theoretical predictions, particularly at high fields.

(2) Three distinctive regions are observed from the I_s-versus-G plot: region I, $I_s \propto G$, $(\tau = \tau_{n0})$; region II, $I_s \propto G^{5/4}$, $(\tau \propto \Delta n^{-1/2})$, and region III, $I_s \propto G^r$, $(r = 2 \sim 2.5)$, $(\tau \propto \Delta n^{-\beta}, \beta = 1\text{–}1.5)$.

(3) The PME open-circuit voltage is found to decrease with increasing temperature as well as with decreasing photoinjection.

(4) The relative photoconductance G/G_0 has a maximum value around 20°K and decreases with either increase or decrease in temperatures.

(5) The PME apparent lifetime τ is decreased with increasing photoinjection and reaches a constant value τ_{n0} at very-high-injection levels.

(6) The high-injection electron lifetime τ_{n0} is found to decrease with decreasing temperature, indicating that the electron-capture cross section is increased with decreasing temperature.

(7) The effect of trapping in regions I and II and for $T > 20$°K can be completely ignored, and the assumption that $\Delta_n = \Delta p$ for these two regions is experimentally verified.

(8) The effective carrier mobility is found to decrease with increasing photoinjection, which can be attributed to the increase in the ionized impurity scattering as the photoinjection is increased.

In addition, the flaw level is believed to be acceptor-type and located in the lower half of the band gap.

ACKNOWLEDGMENT

The author would like to thank C. Wang for his help in taking the experimental data and in preparing the manuscript.

PHYSICAL REVIEW VOLUME 188, NUMBER 3 15 DECEMBER 1969

Dielectric Constant of GaP at 1.6°K

LYLE PATRICK
Westinghouse Research Laboratories, Pittsburgh, Pennsylvania 15235

AND

P. J. DEAN
Bell Telephone Laboratories, Murray Hill, New Jersey 07971

(Received 24 July 1969)

A comparison of observed and calculated line positions in a donor-acceptor pair spectrum yields a value of $\epsilon(0) = 10.75 \pm 0.1$ for the GaP static dielectric constant at 1.6°K. Earlier analyses of pair spectra assumed $\epsilon(0) = 11.1$, the value obtained from Raman-scattering measurements at 300°K. The new value of $\epsilon(0)$ necessitates a small revision in the ionization energies of some donors and acceptors.

I. INTRODUCTION

An accurate value of the static dielectric constant of GaP at room temperature, $\epsilon(0) = 11.1$, has been given by Barker,[1] who combined Raman-scattering results with an extrapolation of Bond's precise measurements[2] of the refractive index for $h\nu > 0.31$ eV. In the absence of reliable information on its temperature dependence, this dielectric constant was used for the analysis of donor-acceptor (DA) spectra measured at 1.6°K.[3,4] Now, however, we show that an accurate fitting of a pair spectrum determines a static dielectric constant of $\epsilon(0) = 10.75 \pm 0.1$ at 1.6°K.

Positive identification of the lines in a DA spectrum requires a consideration of many energy terms. Shell-structure terms depend only on the DA separation.[5] Shell-*substructure* terms depend also on the direction in the lattice from donor to acceptor.[6,7] Some energy terms arise from interactions between the neutral atoms in the *initial* state of the photon-emitting transition. Others arise from Coulomb and multipole interactions in the *final* state. A comparison of observed and calculated line positions is simplified if some of the energy terms are negligible. In this respect the best spectrum now available is that of C+O.[3,6] Our value of the dielectric constant is based on a satisfactory fitting of this spectrum.

II. FITTING C+O SPECTRUM

The C+O spectrum is particularly suitable for the determination of the dielectric constant because three

[1] A. S. Barker, Jr., Phys. Rev. **165**, 917 (1968).
[2] W. L. Bond, J. Appl. Phys. **36**, 1674 (1965).
[3] P. J. Dean, C. H. Henry, and C. J. Frosch, Phys. Rev. **168**, 812 (1968).
[4] P. J. Dean, C. J. Frosch, and C. H. Henry, J. Appl. Phys. **39**, 5631 (1968).
[5] J. J. Hopfield, D. G. Thomas, and M. Gershenzon, Phys. Rev. Letters **10**, 162 (1963).
[6] L. Patrick, Phys. Rev. Letters **21**, 1685 (1968).
[7] L. Patrick, Phys. Rev. **180**, 794 (1969).